



ELSEVIER

1 April 2000

Optics Communications 176 (2000) 281–297

OPTICS
COMMUNICATIONS

www.elsevier.com/locate/optcom

Propagation of a partially coherent beam under the interaction of small and large scales

J. Garnier ^{a,*}, C. Gouédard ^b, L. Videau ^b

^a *Centre de Mathématiques Appliquées, Centre National de la Recherche Scientifique, Unité Mixte de Recherche 7641, Ecole Polytechnique, 91128 Palaiseau Cedex, France*

^b *Commissariat à l'Energie Atomique, Centre d'Etudes Scientifiques et Techniques d'Aquitaine, BP 2, 33114 Le Barp, France*

Received 18 October 1999; received in revised form 17 January 2000; accepted 19 January 2000

Abstract

This paper deals with the propagation of Schell-model sources. Two different and complementary approaches are developed. The first one is standard and based on the study of the Wigner distribution function. The second one follows from a generic statistical representation of the speckle pattern as the superposition of elementary and independent modes. Precise results are obtained for the small- and large-scale characteristics of the beam: optical intensity profile, Rayleigh distance, speckle radius and intensity profiles of the speckle spots. These results are finally applied to the determination of the main characteristics of the focal spot generated by a Kinoform Phase Plate. We also give the complete expressions of the above quantities when the conditions of paraxial approximation are not fulfilled. © 2000 Elsevier Science B.V. All rights reserved.

PACS: 42.25.Kb; 42.60.Jf

Keywords: Speckle statistics; Schell-model sources

1. Introduction

Incoherent light has become a subject of great interest for many applications such as coherent spectroscopy [1], tomography in random media [2] or smoothing techniques for uniform irradiation in plasma physics [3]. This paper has been triggered by the development of optical smoothing techniques for application to Inertial Confinement Fusion (ICF),

which requires a high level of irradiation uniformity for both direct and indirect drive [4]. Spatial beam smoothing is essential in efficient coupling laser energy to ICF targets. It is necessary to generate a focal spot whose energy distribution is a speckled profile that has a flat-top super-Gaussian envelope (8th power or higher) [5]. Binary random phase plates generate a speckled intensity profile with an overall envelope which is an Airy function [6], whose central spot contains only 84% of the total laser energy. So continuous phase screens have been developed which produce a pattern with the same

* Corresponding author. Tel.: +33-1-69-33-46-30; fax: +33-1-69-33-30-11; e-mail: garnier@cmaphx.polytechnique.fr

statistical properties for the fast-varying fluctuations but inside an overall envelope which has super-Gaussian shape [7]. The French Laser MegaJoule [8] or the US National Ignition Facility [9] are designed for the indirect drive scheme, whose principle is that the produced laser energy is focused into a hohlraum and irradiates the gold inner wall to be converted in X-ray. The focal plane of the laser beam is located close to the open hole of the hohlraum, and the beam propagates in the hohlraum from the hole to the inner wall. The typical propagation distance is of the order of a few millimeters.

We aim in this paper at studying the propagation of a beam with speckled intensity profile and at exhibiting the main small- and large-scale features relative to this propagation. Literature contains a lot of work devoted to the propagation of partially coherent beams (see [10] and references therein). Amongst them the Schell model sources characterized by a complex degree of coherence between two points \mathbf{r}_1 and \mathbf{r}_2 in the source plane that depends only on the difference $\mathbf{r}_1 - \mathbf{r}_2$ have attracted attention. In particular Gaussian Schell-model (GSM) sources characterized by Gaussian distributions for both the optical intensity and the complex degree of spatial coherence have been extensively studied [11,12]. This analysis has occurred mainly because the GSM sources can be constructed in the laboratory [13] and are mathematically tractable to provide a relevant insight into the phenomena at hand. Analytical results are restricted mainly to the GSM beams [11], twisted GSM beams [14], J_0 -correlated sources [15] and further incoherent superpositions of Gaussian modes [16]. These results can provide a qualitative insight into the propagation of other kinds of partially coherent beams, but they are not sufficient for our purpose. That is why we shall first derive our results in a very general framework, when the degree of coherence and the overall envelope of the optical intensity have arbitrary profiles and the conditions of paraxial (or Fresnel) approximation are not fulfilled. We shall then apply these results to ICF configurations so as to discuss the two following points. First the super-Gaussian shape will not be preserved along the propagation of the beam, so one cannot expect to have a flat-top envelope at both the open hole and the inner wall. The exact shapes at both planes (which are not parallel) are required for a suitable

design of the hohlraum. Second it is important to have a precise characterization of the hot spots of the beam all along the propagation, since numerical simulations which aim at predicting the growths of plasma instabilities (Rayleigh–Taylor instabilities [17]) strongly depend on the shapes of the hot spots.

The paper is organized as follows. In Section 3 we present and discuss a generic modal representation of a Gaussian field. In Section 4 we study the propagation of the field in the paraxial approximation for some specific models (in particular Gaussian Schell-model sources). We generalize these results to very general configurations in Section 5. Section 6 and Section 7 are specifically devoted to the focal spot generated by a Kinoform Phase Plate (KPP).

2. Formulation

We shall consider in this paper the propagation along the z -axis of a beam with speckled profile and with frequency ω . The real electric field is $\mathcal{E} = 1/2 (Ee^{-i\omega t} + cc)$, and the equation which governs the propagation of the complex field E is the Helmholtz equation:

$$\frac{\partial^2 E}{\partial z^2} + \Delta_{\perp} E + k_0^2 E = 0, \quad (1)$$

where Δ_{\perp} is the Laplacian with respect to the transverse coordinates $\mathbf{r} = (x, y)$ and k_0 is the homogeneous wavenumber. When the typical length scale of characteristic spatial variations of the source is much larger than the carrier wavelength, the paraxial (or Fresnel) approximation holds true and the propagation equation can be simplified into the paraxial wave equation ([18], p. 358):

$$i \frac{\partial \tilde{E}}{\partial z} + \frac{1}{2k_0} \Delta_{\perp} \tilde{E} = 0, \quad (2)$$

$$E = \tilde{E} \exp(ik_0 z). \quad (3)$$

As an initial condition we consider an electric field E_0 in the plane $z = 0$ whose optical intensity profile has a deterministic slowly varying envelope, with spatial radius r_0 , the so-called beam radius. In the experimental conditions corresponding to high power laser chains such as the French Laser MegaJoule [8] or the US National Ignition Facility [9], the beam

radius r_0 is of the order of 250 μm . The beam has also fast-varying random fluctuations, with characteristic scale ρ_0 , the so-called correlation radius. In a typical ICF configuration, ρ_0 is of the order of 2–10 μm . Throughout the paper we consider the asymptotic framework $\rho_0 \ll r_0$ and the statistical analysis is based upon the separation of these scales. We shall assume that the fast-varying modulations of the beam obey Gaussian statistics. In particular the spatial intensity distribution is a speckle pattern [19], and the field is a Schell-model source [10]. These statistical characteristics are actually very usual, and correspond to the pulses generated by the smoothing techniques that we quote here above [20]. The statistical distribution is characterized in the plane $z = 0$ by the Cross Autocorrelation Function (CAF) defined by:

$$\gamma_0(\mathbf{r}, \boldsymbol{\rho}) := \left\langle E_0\left(\mathbf{r} + \frac{\boldsymbol{\rho}}{2}\right) E_0^*\left(\mathbf{r} - \frac{\boldsymbol{\rho}}{2}\right) \right\rangle, \quad (4)$$

where $\langle \cdot \rangle$ stands for an ensemble average. Ensemble averages make sense in the framework $\rho_0 \ll r_0$. Indeed, let us define the auxiliary CAF through the spatial average:

$$\begin{aligned} \tilde{\gamma}_0^D(\mathbf{r}, \boldsymbol{\rho}) &:= \\ &= \frac{1}{|D|} \int_D E_0\left(\mathbf{r} + \frac{\boldsymbol{\rho}}{2} + \mathbf{r}'\right) E_0^*\left(\mathbf{r} - \frac{\boldsymbol{\rho}}{2} + \mathbf{r}'\right) d^2 \mathbf{r}' \end{aligned} \quad (5)$$

over the disc D with center at 0 and radius $\sqrt{\rho_0 r_0}$. The dimension of this domain is small compared with r_0 , so that the statistics of the field is stationary over D , and large compared with ρ_0 , so that spatial ergodicity holds true and makes the CAF defined through the ensemble average (4) coincide with the CAF defined through the spatial average (5). The CAF of a Schell-model source is of the form ([10], p. 234):

$$\begin{aligned} \gamma_0(\mathbf{r}, \boldsymbol{\rho}) &:= \\ &= g^{1/2}\left(\frac{\mathbf{r}}{r_0} + \frac{\boldsymbol{\rho}}{2r_0}\right) g^{1/2}\left(\frac{\mathbf{r}}{r_0} - \frac{\boldsymbol{\rho}}{2r_0}\right) f\left(\frac{\boldsymbol{\rho}}{\rho_0}\right), \end{aligned} \quad (6)$$

where f is the degree of coherence ($f(\mathbf{0}) = 1$), and g the overall envelope of the optical intensity profile.

We may think at a super-Gaussian shape:

$$g(\bar{\mathbf{r}}) = I_0 \exp(-|\bar{\mathbf{r}}|^n).$$

I_0 is then the mean intensity at the beam center and n is the power of the super-Gaussian shape. This envelope is Gaussian if $n = 2$ and strictly super-Gaussian if $n = 4, 6, \dots$. We consider a particular class of Schell-model sources, namely those for which the envelope $g(\cdot/r_0)$ varies so slowly (at scale r_0) with position that it is approximately constant over distances across the source that are of the order of the correlation radius ρ_0 . In addition we also assume that r_0 is much larger than the carrier wavelength λ_0 . Schell-model sources of this kind are known as quasi-homogeneous sources. Note that we do not require that ρ_0 be much larger than λ_0 . Since the envelope $g(\cdot/r_0)$ is assumed to vary slowly with position over the effective width ρ_0 of $f(\cdot/\rho_0)$, we may make on the right-hand side of Eq. (6) the usual approximation:

$$g^{1/2}\left(\frac{\mathbf{r}}{r_0} + \frac{\boldsymbol{\rho}}{2r_0}\right) \approx g^{1/2}\left(\frac{\mathbf{r}}{r_0} - \frac{\boldsymbol{\rho}}{2r_0}\right) \approx g^{1/2}\left(\frac{\mathbf{r}}{r_0}\right)$$

Using this approximation in Eq. (6) we see that the CAF of a quasi-homogeneous source may be expressed as ([10], p. 235):

$$\gamma_0(\mathbf{r}, \boldsymbol{\rho}) = g\left(\frac{\mathbf{r}}{r_0}\right) f\left(\frac{\boldsymbol{\rho}}{\rho_0}\right). \quad (7)$$

We shall be interested in the following in the evolution along the propagation of the CAF γ_z defined by:

$$\gamma_z(\mathbf{r}, \boldsymbol{\rho}) := \left\langle E\left(z, \mathbf{r} + \frac{\boldsymbol{\rho}}{2}\right) E^*\left(z, \mathbf{r} - \frac{\boldsymbol{\rho}}{2}\right) \right\rangle. \quad (8)$$

This function contains much relevant information. In particular it gives the global radius of the optical intensity profile since $\mathbf{r} \mapsto \gamma_z(\mathbf{r}, \mathbf{0})$ is precisely the overall envelope of the optical intensity profile. Furthermore we shall determine the Three-Dimensional Autocorrelation Function (3DAF):

$$\begin{aligned} \gamma_z(\mathbf{r}, \boldsymbol{\rho}, \boldsymbol{\zeta}) &:= \\ &:= \left\langle E\left(z + \frac{\boldsymbol{\zeta}}{2}, \mathbf{r} + \frac{\boldsymbol{\rho}}{2}\right) E^*\left(z - \frac{\boldsymbol{\zeta}}{2}, \mathbf{r} - \frac{\boldsymbol{\rho}}{2}\right) \right\rangle. \end{aligned} \quad (9)$$

This function describes the typical three-dimensional shapes of the speckle spots of the beam. Indeed

well-known results on Gaussian processes (see Adler [21]) establish that the typical behavior of the field around a local maximum located at situ (Z, \mathbf{R}) is precisely given by the function $(\boldsymbol{\rho}, \zeta) \mapsto \gamma_Z(\mathbf{R}, \boldsymbol{\rho}, \zeta)$:

$$|E(Z + \zeta, \mathbf{R} + \boldsymbol{\rho})| \approx |E(Z, \mathbf{R})| \frac{|\gamma_Z(\mathbf{R}, \boldsymbol{\rho}, \zeta)|}{|\gamma_Z(\mathbf{R}, \mathbf{0}, 0)|}. \quad (10)$$

This result holds true for values of $(\boldsymbol{\rho}, \zeta)$ small enough so that the right-hand side is larger than $\sqrt{I_0}$.

3. Modal representation of a field with Gaussian statistics

3.1. Speckle pattern with flat envelope

A field E with stationary Gaussian statistics can be represented by a superposition of simple and statistically independent modes. Indeed, by the central limit theorem, the Gaussian statistics results from the superposition of numerous elementary fields. In some points, this superposition is destructive by interference, and in other points, the so-called hot spots or speckle spots, this superposition is constructive. Within this viewpoint we are going to give a universal representation of a field E with stationary Gaussian statistics. At the expense of a straightforward rescaling, we may assume that E has zero-mean. The field E is then characterized by the CAF:

$$\langle E(\mathbf{r}) E^*(\mathbf{r}') \rangle = I_0 f\left(\frac{\mathbf{r} - \mathbf{r}'}{\rho_0}\right),$$

where f is a function whose modulus is bounded above by 1 and which satisfies $f(\mathbf{0}) = 1$. The following proposition is an elementary statement which will play the role of a basis for the forthcoming results.

Proposition 1: The field E can be represented by the sum of the modes $(E_j)_{j=1, \dots, N}$, with $N \gg 1$ and:

$$E_j(\mathbf{r}) = \frac{\sqrt{I_0}}{\sqrt{N}} \exp i\left(\frac{\mathbf{a}_j \cdot \mathbf{r}}{\rho_0} + \phi_j\right), \quad (11)$$

where $\mathbf{r} \cdot \mathbf{r}'$ stands for the usual scalar product in \mathbb{R}^2 , the ϕ_j 's are random phases, statistically independent and chosen uniformly over $[0, 2\pi]$, and $1/\sqrt{N}$ is the weight of the j th mode in the superposition. The

\mathbf{a}_j 's are \mathbb{R}^2 -valued random variables independent and identically distributed. They obey the distribution whose density with respect to the Lebesgue measure over \mathbb{R}^2 is the inverse Fourier transform $\hat{f}(\mathbf{a})$ of the function f :

$$\hat{f}(\mathbf{a}) = \frac{1}{(2\pi)^2} \int_{\mathbb{R}^2} e^{-i\mathbf{a} \cdot \bar{\mathbf{r}}} f(\bar{\mathbf{r}}) d\bar{\mathbf{r}}. \quad (12)$$

Note that in view of the Wiener–Khinchine theorem [22], \hat{f} is proportional to the power spectral density of the stationary field E and is consequently nonnegative.

Proof: Let us consider the sum:

$$E^N(\mathbf{r}) := \frac{\sqrt{I_0}}{\sqrt{N}} \sum_{j=1}^N \exp i\left(\frac{\mathbf{a}_j \cdot \mathbf{r}}{\rho_0} + \phi_j\right). \quad (13)$$

The modes are statistically independent, so the central limit theorem can be applied which yields that E^N converges, as $N \rightarrow \infty$, to a process with Gaussian distribution, zero-mean and correlation function:

$$\begin{aligned} K(\mathbf{r}, \mathbf{r}') &= I_0 \left\langle \exp i\left(\mathbf{a}_1 \cdot \frac{\mathbf{r} - \mathbf{r}'}{\rho_0}\right) \right\rangle \\ &= I_0 \int_{\mathbb{R}^2} \exp i\left(\mathbf{a} \cdot \frac{\mathbf{r} - \mathbf{r}'}{\rho_0}\right) \hat{f}(\mathbf{a}) d^2 \mathbf{a} \end{aligned}$$

This correlation function depends only on the difference $\mathbf{r} - \mathbf{r}'$, which proves that the limit field is statistically stationary. Furthermore K is the direct Fourier transform of \hat{f} , that is to say the function f . Since a field with Gaussian statistics is fully characterized by its first and second moments, this completes the proof of the proposition.

The modes we describe in Proposition 1 are nothing else but a discrete set of plane waves with random phases ϕ_j and random transverse wavevectors \mathbf{k}_j chosen according to the distribution with density $\hat{f}(\mathbf{k}_j \rho_0)$. Let us cite two relevant examples that will be encountered in the following sections:

- If $f(\bar{\mathbf{r}}) = \exp(-|\bar{\mathbf{r}}|^2)$, then \mathbf{a} obeys a normal distribution with density:

$$\hat{f}(\mathbf{a}) = \frac{1}{4\pi} \exp -\frac{|\mathbf{a}|^2}{4}.$$

- If $f(\bar{\mathbf{r}}) = 2J_1(\pi|\bar{\mathbf{r}}|)/(\pi|\bar{\mathbf{r}}|)$, then \mathbf{a} obeys the uniform distribution over the disc $B(0, \pi)$ with cen-

ter at 0 and radius π . The density of this distribution with respect to the Lebesgue measure over \mathbb{R}^2 is:¹

$$\hat{f}(\mathbf{a}) = \pi^{-3} \chi_{B(0,\pi)}(\mathbf{a}).$$

3.2. Generalization to a speckle pattern with a slowly varying overall envelope

Let us now consider that the field E is locally stationary in the sense that it possesses an overall envelope with radius $r_0 \gg \rho_0$, so that its CAF is (6).

Proposition 2. The field E can be represented by the sum of the modes $(E_j)_{j=1,\dots,N}$, with $N \gg 1$ and:

$$E_j(\mathbf{r}) = \frac{1}{\sqrt{N}} \exp i \left(\frac{\mathbf{a}_j \cdot \mathbf{r}}{\rho_0} + \phi_j \right) g^{1/2} \left(\frac{\mathbf{r}}{r_0} \right), \quad (14)$$

where the ϕ_j 's and \mathbf{a}_j 's are as described in Proposition 1.

Proof: The arguments are the same as here above. By the central limit theorem, the superposition converges as $N \rightarrow \infty$ to a field with Gaussian statistics, zero-mean and CAF (6), which proves the desired result.

4. Propagation in the paraxial approximation

A speckle pattern is a field with Gaussian statistics, whose contrast² is therefore equal to 1. In this section we assume that the conditions of paraxial approximation are satisfied, that is to say $k_0 \rho_0 \gg 1$. Diffraction is linear, so the Gaussian property of the statistics is conserved along the propagation. As a consequence, for any z , the field $E(z)$ which results from the propagation of E_0 over a distance z is still a speckle pattern, with contrast 1, and its CAF defined by (8) is solution of:

$$i \frac{\partial \gamma_z}{\partial z} + \frac{1}{k_0} \nabla_{\mathbf{r}} \cdot \nabla_{\boldsymbol{\rho}} \gamma_z = 0, \quad (15)$$

where $\mathbf{r} = (x, y)$ and $\boldsymbol{\rho} = (\rho_x, \rho_y)$. The usual way to solve this equation consists in introducing the Wigner

distribution defined as the Fourier transform with respect to $\boldsymbol{\rho}$ of the CAF [23]:

$$W_z(\mathbf{r}, \mathbf{k}) = \int \gamma_z(\mathbf{r}, \boldsymbol{\rho}) e^{i\mathbf{k} \cdot \boldsymbol{\rho}} d^2 \boldsymbol{\rho}. \quad (16)$$

One can recover the CAF by an inverse Fourier transform. From Eq. (15) it is easy to establish the equation which governs the evolution of the Wigner distribution:

$$k_0 \frac{\partial W_z}{\partial z} - \mathbf{k} \cdot \nabla_{\mathbf{r}} W_z = 0. \quad (17)$$

We thus obtain the well-known property that the Wigner distribution is transported along the rays defined by the law of geometric optics, although it contains all the information of diffraction [24]. The solution of the transport Eq. (17) simply writes:

$$W_z(\mathbf{r}, \mathbf{k}) = W_0 \left(\mathbf{r} + \mathbf{k} \frac{z}{k_0}, \mathbf{k} \right). \quad (18)$$

By an inverse Fourier transform we then get that the CAF in the plane at distance z is given by:

$$\gamma_z(\mathbf{r}, \boldsymbol{\rho}) = \frac{1}{(2\pi)^2} \int W_0 \left(\mathbf{r} + \mathbf{k} \frac{z}{k_0}, \mathbf{k} \right) e^{-i\mathbf{k} \cdot \boldsymbol{\rho}} d^2 \mathbf{k}. \quad (19)$$

The Wigner transform thus appears efficient to compute the CAF, but it does not give an insight of the 3DAF. Although we could introduce a three-dimensional Wigner function, we shall see that the modal representation provides an easy way to compute the 3DAF.

4.1. Speckle pattern with flat envelope

We consider an input speckle pattern E_0 whose statistics is spatially stationary over the whole plane $z = 0$, (i.e. $r_0 = \infty$) with correlation radius ρ_0 . The CAF of the input field E_0 defined by (4) is in this configuration:

$$\gamma_0(\mathbf{r}, \boldsymbol{\rho}) = I_0 f \left(\frac{\boldsymbol{\rho}}{\rho_0} \right). \quad (20)$$

Whatever z , the field $E(z)$ which results from the propagation of E_0 over a distance z is a speckle pattern and its CAF is solution of (15), and is consequently identically equal to γ_0 . As a conclusion, the statistical distribution of the field is the same for any z .

¹ Throughout the paper we denote by χ_A the characteristic function of the set A , that is to say $\chi_A(x) = 1$ if $x \in A$ and 0 otherwise.

² The contrast is defined as the ratio of the variance of the intensity over the mean intensity. It is a parameter which characterizes the relative fluctuations of the intensity of a random field with respect to its mean value.

In order to compute the 3DAF we consider the modal representation (11). We can compute explicitly the propagation of every mode and find their exact expressions for any z . The input field E_0 can be represented by the superposition of the modes $(E_j)_{j=1,\dots,N}$, with $N \gg 1$ and:

$$E_j(\mathbf{r}) = \frac{\sqrt{I_0}}{\sqrt{N}} \exp i \left(\frac{\mathbf{a}_j \cdot \mathbf{r}}{\rho_0} + \phi_j \right), \quad (21)$$

where the ϕ_j 's are random phases, statistically independent and chosen uniformly over $[0, 2\pi]$, the \mathbf{a}_j 's are \mathbb{R}^2 -valued random variables independent and identically distributed according to the distribution whose density \hat{f} with respect to the Lebesgue measure over \mathbb{R}^2 is given by (12). The fields $E(z)$ after propagation over a distance z is then given by the superposition of the diffracted modes $(E_j(z))_{j=1,\dots,N}$, with:

$$E_j(z, \mathbf{r}) = \frac{\sqrt{I_0}}{\sqrt{N}} \exp i \left(\frac{\mathbf{a}_j \cdot \mathbf{r}}{\rho_0} + \phi_j(z) \right), \quad (22)$$

where the phases $\phi_j(z)$ are imposed by Eq. (2):

$$\phi_j(z) = \phi_j + k_0 z - \frac{z}{4\zeta_0} |\mathbf{a}_j|^2, \quad (23)$$

with $\zeta_0 = k_0 \rho_0^2 / 2$. Whatever z , the phases $\phi_j(z)$ obey the same distributions as the initial phases ϕ_j , that is to say independent and uniform distributions over $[0, 2\pi]$. However, as soon as $z \geq \zeta_0$, the phase mismatches $\phi_j(z) - \phi_j$ are not equal to $\phi_j - \phi_j$ anymore, neither is $E(z)$ equal to E_0 . After a propagation distance $z \geq \zeta_0$, the statistical distribution of the modes is unchanged, but the modes have changed. One can say that we deal with a new realization of the same distribution. The superposition of the modes is governed by the same rules, but the points where the superposition is destructive or constructive are not the same anymore. Thus, the field $E(z)$ has the same statistical distribution as the field E_0 (same contrast, same type of hot spots), but it is a new speckle pattern. As a conclusion, whatever z , the field $E(z)$ is a pattern with hot spots with radius ρ_0 , but the spots move every $\zeta_0 = k_0 \rho_0^2 / 2$.

We can study more precisely the modification of the field along the z -axis by considering the 3DAF.

Using the modal representation, the 3DAF reads as a double sum over j and j' of terms $\langle E_j E_{j'}^* \rangle$. The contributions of the crossed terms $\langle E_j E_{j'}^* \rangle$ for $j \neq j'$ vanish due to the random phases ϕ_j . It remains only the diagonal terms $\langle E_j E_j^* \rangle$ which are equal, which establishes that:

$$\begin{aligned} \gamma_z(\mathbf{r}, \boldsymbol{\rho}, \zeta) &= N \left\langle E_1 \left(z + \frac{\zeta}{2}, \mathbf{r} + \frac{\boldsymbol{\rho}}{2} \right) E_1^* \left(z - \frac{\zeta}{2}, \mathbf{r} - \frac{\boldsymbol{\rho}}{2} \right) \right\rangle. \end{aligned}$$

It thus appears that it is sufficient to compute the 3DAF of a single mode to get the 3DAF of the total field. The first quantity is of course much simpler to compute in view of the simple form of the mode. This method to compute the 3DAF will be applied to more general configurations in the forthcoming sections. Here we find that the 3DAF does not depend on \mathbf{r} and z and can be expressed as:

$$\begin{aligned} \gamma_z(\mathbf{r}, \boldsymbol{\rho}, \zeta) &= I_0 \int_{\mathbb{R}^2} \exp i \left(\frac{\mathbf{a} \cdot \boldsymbol{\rho}}{\rho_0} - \frac{|\mathbf{a}|^2 \zeta}{4\zeta_0} \right) \hat{f}(\mathbf{a}) d\mathbf{a} \exp(ik_0 \zeta). \end{aligned}$$

In case of a Gaussian degree of coherence, that is to say $f(\bar{\boldsymbol{\rho}}) = \exp -|\bar{\boldsymbol{\rho}}|^2$, the 3DAF reads:

$$\begin{aligned} \gamma_z(\mathbf{r}, \boldsymbol{\rho}, \zeta) &= \frac{I_0}{\sqrt{1 + \beta^2(\zeta)}} \\ &\times \exp \left(-\frac{|\boldsymbol{\rho}|^2}{\rho_0^2 (1 + \beta^2(\zeta))} + i\psi(\zeta, \boldsymbol{\rho}) \right), \\ \psi(\zeta, \boldsymbol{\rho}) &= k_0 \zeta - \arctan(\beta(\zeta)) - \frac{|\boldsymbol{\rho}|^2}{\rho_0^2} \frac{\beta(\zeta)}{1 + \beta^2(\zeta)}, \end{aligned} \quad (24a)$$

$$\beta(\zeta) = \frac{\zeta}{\zeta_0}, \quad \zeta_0 = \frac{k_0 \rho_0^2}{2}, \quad (24b)$$

which confirms that for $\zeta > \zeta_0$, the fields in two planes separated by ζ are uncorrelated, that is to say different, although they obey the same statistical distribution.

4.2. Gaussian Schell-model source

Let us consider a speckle pattern E_0 with correlation radius ρ_0 whose overall envelope has radius r_0 (with $\rho_0 \ll r_0$). The statistics are then only locally stationary, so the above derived results will hold true only locally. The CAF of the input field E_0 is assumed to correspond to a Gaussian Schell model source so it reads:

$$\gamma_0(\mathbf{r}, \boldsymbol{\rho}) = I_0 \exp\left(-\frac{|\mathbf{r}|^2}{r_0^2} - \frac{|\boldsymbol{\rho}|^2}{\rho_0^2}\right). \quad (25)$$

We still assume in this section that $k_0 \rho_0 \gg 1$ so that the paraxial approximation holds true and the propagation is governed by paraxial wave Eq. (2).

4.2.1. Cross autocorrelation function

We denote by $E(z)$ the field which results from the paraxial propagation of E_0 over a distance z , which is a speckle pattern with contrast 1, whose CAF is solution of Eq. (15) and is consequently given by:

$$\begin{aligned} \gamma_z(\mathbf{r}, \boldsymbol{\rho}) &= \frac{I_0}{w(z)} \\ &\times \exp\left(-\frac{|\mathbf{r}|^2}{r_0^2 w(z)} - \frac{|\boldsymbol{\rho}|^2}{\rho_0^2 w(z)} + i\psi_z(\mathbf{r}, \boldsymbol{\rho})\right), \\ \psi_z(\mathbf{r}, \boldsymbol{\rho}) &= \frac{4z}{z_0 w(z)} \frac{\mathbf{r} \cdot \boldsymbol{\rho}}{r_0 \rho_0}, \\ w(z) &= 1 + \frac{4z^2}{z_0^2}, \quad z_0 = k_0 r_0 \rho_0. \end{aligned} \quad (26)$$

This expression is well-known and was derived previously in [11]. It thus appears that the propagation distance for which evolutions of the shapes of the global envelope and of the speckle spots are noticeable is of the order of $k_0 \rho_0 r_0 / 2$. Note that this distance is equal to the geometric average of the natural Rayleigh distance $k_0 \rho_0^2 / 2$ corresponding to a coherent beam with radius ρ_0 (the scale of the fast-varying fluctuations) and of the natural Rayleigh distance $k_0 r_0^2 / 2$ corresponding to a coherent beam with radius r_0 (the scale of the overall envelope).

4.2.2. Modal approach

The input field E_0 can be represented by the superposition of the modes $(E_j)_{j=1, \dots, N}$ given by (21) with an overall envelope with Gaussian shape:

$$E_j(\mathbf{r}) = \frac{\sqrt{I_0}}{\sqrt{N}} \exp i\left(\frac{\mathbf{a}_j \cdot \mathbf{r}}{\rho_0} + \phi_j\right) \exp -\frac{|\mathbf{r}|^2}{2r_0^2}. \quad (27)$$

After propagation over a distance z , the field $E(z)$ is given by the superposition of the modes $(E_j(z))_{j=1, \dots, N}$ whose expressions can be computed explicitly:

$$\begin{aligned} E_j(z, \mathbf{r}) &= \frac{\sqrt{I_0}}{\sqrt{N\chi(z)}} \\ &\times \exp i\left(\frac{\mathbf{a}_j \cdot \mathbf{r}}{\rho_0 \chi(z)} + \phi_j(z) - \frac{|\mathbf{r}|^2}{2r_0^2 \chi(z)} \right. \\ &\left. + \frac{z}{z_0} \frac{\mathbf{a}_j \cdot \mathbf{r}}{r_0 \chi(z)} - \frac{z^2}{z_0^2} \frac{|\mathbf{a}_j|^2}{2\chi(z)}\right), \\ \phi_j(z) &= \phi_j + k_0 z - \frac{z}{4\xi_0} \frac{|\mathbf{a}_j|^2}{\chi(z)} \\ &+ \frac{z}{2k_0 r_0^2 \chi(z)} \frac{|\mathbf{r}|^2}{r_0^2} - \arctan\left(\frac{z}{k_0 r_0^2}\right), \end{aligned} \quad (28)$$

where $\chi(z) = 1 + z^2 / (k_0^2 r_0^4)$. By neglecting the terms of order $z / (k_0 r_0^2)$, this expression simplifies:

$$\begin{aligned} E_j(z, \mathbf{r}) &= \frac{\sqrt{I_0}}{\sqrt{N}} \exp i\left(\frac{\mathbf{a}_j \cdot \mathbf{r}}{\rho_0} + \phi_j(z) - \frac{|\mathbf{r}|^2}{2r_0^2} \right. \\ &\left. + \frac{z}{z_0} \frac{\mathbf{a}_j \cdot \mathbf{r}}{r_0} - \frac{z^2}{2z_0^2} |\mathbf{a}_j|^2\right), \end{aligned} \quad (29)$$

with $\phi_j(z) = \phi_j + k_0 z - |\mathbf{a}_j|^2 z / (4\xi_0)$. We thus put into evidence that the influence of the envelope consists in two terms (the two last terms of Eq. (29)) which affect the amplitudes of the modes after a propagation distance of the order of $z_0 = k_0 r_0 \rho_0$. After this distance, the modes obey a different distribution, the superposition does not obey the same rules which modifies the total field E .

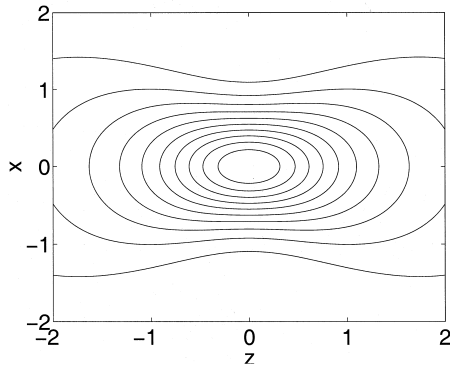


Fig. 1. Normalized contour plot (maximum set to 1, and lines scaled by 0.1) of the intensity of the field around a local maximum located close to the plane $Z = 0$. The z -scale is a multiple of ζ_0 , while the x -scale is a multiple of ρ_0 .

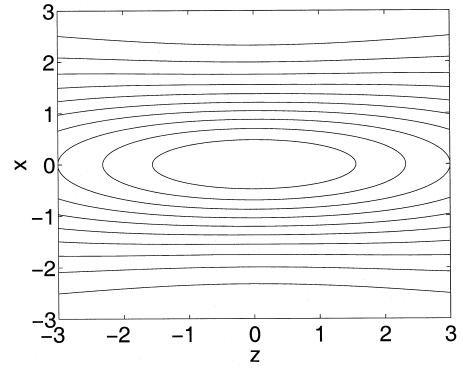


Fig. 2. The same as in Fig. 1 for a local maximum located close to the point $Z = z_0$, $\mathbf{R} = (0,0)$.

4.2.3. *Three-dimensional autocorrelation function*

We can fully characterize the evolution of the field by studying the 3DAF. By the arguments developed in Section 4 the 3DAF of the field E is equal to the 3DAF of the mode E_1 . Some algebra based on integrals of Gaussian functions then establishes that:

$$\begin{aligned} \gamma_z(\mathbf{r}, \boldsymbol{\rho}, \zeta) &= \frac{I_0}{\sqrt{w^2(z) + \beta^2(\zeta)}} \\ &\times \exp\left(-\frac{|\mathbf{r}|^2}{r_0^2} \frac{w(z) + \beta^2(\zeta)}{w^2(z) + \beta^2(\zeta)} - \frac{|\boldsymbol{\rho}|^2}{\rho_0^2} \frac{w(z)}{w^2(z) + \beta^2(\zeta)}\right) \\ &\times \exp\left(\frac{2\mathbf{r} \cdot \boldsymbol{\rho}}{r_0 \rho_0} \frac{\beta(\zeta) \sqrt{w(z) - 1}}{w^2(z) + \beta^2(\zeta)}\right) \\ &\times \exp i \psi_z(\mathbf{r}, \boldsymbol{\rho}, \zeta), \\ \psi_z(\mathbf{r}, \boldsymbol{\rho}, \zeta) &= k_0 \zeta - \arctan\left(\frac{\beta(\zeta)}{w(z)}\right) \\ &+ \frac{2\mathbf{r} \cdot \boldsymbol{\rho}}{r_0 \rho_0} \frac{w(z) \sqrt{w(z) - 1}}{w^2(z) + \beta^2(\zeta)^2} \\ &- \frac{\beta(\zeta)}{w^2(z) + \beta^2(\zeta)^2} \\ &\times \left((w(z) - 1) \frac{|\mathbf{r}|^2}{r_0^2} - \frac{|\boldsymbol{\rho}|^2}{\rho_0^2} \right) \end{aligned}$$

where $\beta(\zeta)$ and $w(z)$ are defined by (24b) and (26) respectively. This closed-form expression provides an accurate insight into the shapes of the speckle spots according to Adler’s theorem (10). Figs. 1–3 are contour plots of the functions:

$$(x, z) \mapsto \frac{|\gamma_z(\mathbf{R}, (x,0), z)|^2}{|\gamma_z(\mathbf{R}, \mathbf{0}, 0)|^2}$$

in different points (\mathbf{R}, Z) . They give the shapes of the intensity profiles of the speckle spots located at distance Z from the source plane and at situ \mathbf{R} from the beam center. When Z becomes of order z_0 , the hot spots become larger (Fig. 2), and the spots which are located at the edges of the overall envelope are no more directed along the z -axis, but along the

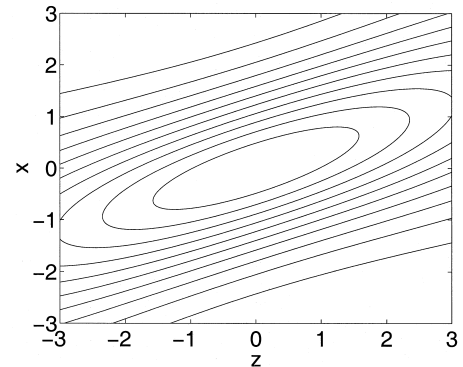


Fig. 3. The same as in Fig. 1 for a local maximum located close to the point $Z = z_0$, $\mathbf{R} = (r_0, 0)$. The vector along which the speckle spot is directed is $(\mathbf{e}_s(\mathbf{R}, Z), \zeta_0) = ((\sqrt{3})/4)\rho_0, 0, \zeta_0$.

direction imposed by the vector $(\mathbf{e}_s(\mathbf{R}, Z), \zeta_0)$ of \mathbb{R}^3 where \mathbf{e}_s is the field of vectors of \mathbb{R}^2 defined by:

$$\mathbf{e}_s(\mathbf{R}, Z) = \rho_0 \frac{\sqrt{w(Z) - 1}}{w(Z)} \frac{\mathbf{R}}{r_0}.$$

Fig. 3 is an example of this feature, which can be also put into evidence by setting

$$\tilde{\boldsymbol{\rho}} = \frac{\boldsymbol{\rho} + \beta(\zeta) \mathbf{e}_s(\mathbf{r}, z)}{\sqrt{1 + \beta(\zeta)^2 w^{-2}(z)}}$$

in the expression of the 3DAF, so that its square modulus reads:

$$|\gamma_z(\mathbf{r}, \boldsymbol{\rho}, \zeta)|^2 = \frac{I_0^2}{w^2(z) + \beta^2(\zeta)} \times \exp\left(-\frac{2|\mathbf{r}|^2}{r_0^2 w(z)} - \frac{2|\tilde{\boldsymbol{\rho}}|^2}{\rho_0^2 w(z)}\right).$$

The speckle spots seem to follow the curvature of the overall envelope. The schematic view of Fig. 13 describes the arrangements of the speckle spots in a partially coherent beam.

Note that we have just dealt with the propagation in the paraxial approximation of a speckle pattern with flat envelope on the one hand (Section 4.1) and of a Gaussian Schell-model source (Section 4.2). The propagation in the paraxial approximation of a general Schell-model source will be addressed in Section 5.3 as an application of the general results that will be derived in the next Section.

5. Propagation governed by the Helmholtz equation

We consider in this section the general form (7) for the CAF of the input beam. The inverse Fourier transform \hat{f} defined by (12) of the degree of coherence f will play a crucial role. We shall moreover use the inverse Fourier transform of the overall envelope:

$$\hat{g}(\mathbf{u}) = \frac{1}{4\pi^2} \int_{\mathbb{R}^2} g(\bar{\mathbf{r}}) e^{-i\bar{\mathbf{r}} \cdot \mathbf{u}} d^2 \bar{\mathbf{r}}. \tag{30}$$

The problem at hand is the study of the small- and large-scale properties of the beam along free propa-

gation. We shall consider a more general propagation equation than the paraxial wave Eq. (2) which is derived under the paraxial approximation. Indeed this approximation is valid when $\rho_0 \gg \lambda_0$. In this section we only assume that $\rho_0 \geq \lambda_0$. The general equation which governs the propagation of the field is then the Helmholtz Eq. (1).

5.1. Speckle pattern with flat envelope

We first restrict ourselves to the case of stationary fields with flat envelopes. In other words we assume that the pattern in the plane $z = 0$ has stationary Gaussian statistics with degree of coherence f , whose Fourier transform is \hat{f} . The field in the plane $z = 0$ can then be represented by the superposition of modes

$$E_j(\mathbf{r}) = \frac{\sqrt{I_0}}{\sqrt{N}} \exp i\left(\frac{\mathbf{a}_j \cdot \mathbf{r}}{\rho_0} + \phi_j\right),$$

where the ϕ_j are independent random variables with uniform distribution over $[0, 2\pi]$, and the \mathbf{a}_j 's are independent random variables whose distributions have the density \hat{f} with respect to the Lebesgue measure over \mathbb{R}^2 . The expressions of the modes out of the initial plane $z = 0$ are imposed by Eq. (1):

$$E_j(\mathbf{r}, z) = \frac{\sqrt{I_0}}{\sqrt{N}} \exp i\left(\frac{\mathbf{a}_j \cdot \mathbf{r}}{\rho_0} + \phi_j(z)\right), \tag{31a}$$

$$\phi_j(z) = z \sqrt{k_0^2 - \frac{|\mathbf{a}_j|^2}{\rho_0^2}}. \tag{31b}$$

For those j whose $|\mathbf{a}_j|^2$ is larger than $k_0 \rho_0$, the root in (31b) should be taken with a positive imaginary part. The corresponding eigenmode is then evanescent. By the arguments developed in Section 4 the 3DAF of the field E is equal to the 3DAF of the mode E_1 . Consequently the 3DAF of the total field E is stationary and given by:

$$\gamma(\boldsymbol{\rho}, \zeta) = I_0 \int_{B(0, P)} \exp i\left(\frac{\mathbf{u} \cdot \boldsymbol{\rho}}{\rho_0} + \zeta \sqrt{k_0^2 - \frac{|\mathbf{u}|^2}{\rho_0^2}}\right) \times \hat{f}(\mathbf{u}) d^2 \mathbf{u},$$

where $P = k_0 \rho_0$. To study the longitudinal form of the 3DAF $\zeta \mapsto \gamma(\boldsymbol{\rho} = \mathbf{0}, \zeta)$, let us consider a specific example and assume that $f(\bar{\mathbf{r}}) = 2J_1(\pi|\bar{\mathbf{r}}|)/(\pi|\bar{\mathbf{r}}|)$ so that $\hat{f}(\mathbf{u}) = \pi^{-3}\chi_{B(0,\pi)}(\mathbf{u})$. Denoting $\bar{P} = P/\pi$ and $\zeta_0 = k_0 \rho_0^2/2$, we get:

$$|\gamma(\boldsymbol{\rho} = \mathbf{0}, \zeta)|^2 = I_0^2 F_{\bar{P}} \left(\frac{\pi^2 \zeta}{2 \zeta_0} \right),$$

$$F_{\bar{P}}(\bar{\zeta}) = 4\bar{\zeta}^{-2}(2 - \bar{P}^{-2}) - 8\bar{\zeta}^{-3}\bar{P}^{-4}\sin(\alpha_p \bar{\zeta})\alpha_p$$

$$+ 8\bar{P}^{-6}\cos(\alpha_p \bar{\zeta})\bar{\zeta}^{-2}(\bar{P}^2 - \alpha_p)$$

$$+ 8\bar{P}^{-4}\bar{\zeta}^{-3}(1 - \cos(\alpha_p \bar{\zeta})) \quad (32)$$

where $\alpha_p = \bar{P}^2(1 - \sqrt{1 - \bar{P}^{-2}})$. In the paraxial approximation $\bar{P} \gg 1$ we have in this configuration:

$$|\gamma(\boldsymbol{\rho} = \mathbf{0}, \zeta)|^2|_{\text{parax}} = I_0^2 \text{sinc}^2 \left(\frac{\pi \zeta}{8 \zeta_0} \right), \quad (33)$$

where $\text{sinc}(s) = \sin(\pi s)/(\pi s)$. Comparing the curves plotted in Fig. 4 it appears that the paraxial approximation tends to enhance the true longitudinal length of the speckle spots.

5.2. Speckle pattern with envelope

The field in the plane $z = 0$ is the superposition of the modes:

$$E_j(\mathbf{r}) = \frac{1}{\sqrt{N}} \exp i \left(\frac{\mathbf{a}_j \cdot \mathbf{r}}{\rho_0} + \phi_j \right) g^{1/2} \left(\frac{\mathbf{r}}{r_0} \right).$$

The propagation of the mode E_j is governed by the Helmholtz Eq. (1). In order to establish the expression of the mode E_j for propagation distances of the order $z/(k_0 r_0 \rho_0)$, we shall follow a standard method which is based on high-frequency expansions of the solutions of partial differential equations. We introduce the small parameter $\delta = \rho_0/r_0$ and we seek the solution in the form:

$$E_j(z, \mathbf{r}) = U_j(z, \mathbf{r}) \exp i \left(\frac{\mathbf{a}_j \cdot \mathbf{r}}{\rho_0} + k_j z \right),$$

where k_j is a real to be determined, U_j can be expanded as:

$$U_j(z, \mathbf{r}) = \sum_{n=0}^{\infty} \delta^n u_{j,n} \left(\delta \frac{z}{\zeta_0}, \delta \frac{\mathbf{r}}{\rho_0} \right), \quad (34)$$

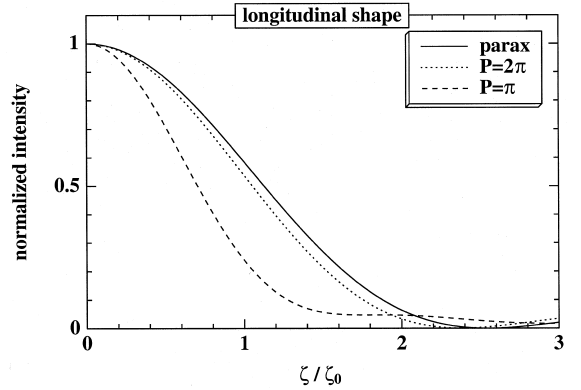


Fig. 4. Normalized longitudinal shape of the intensity profile of a speckle spot. The paraxial configuration is plotted in solid line; it corresponds to the limit case $P \rightarrow \infty$ and is given by formula (33). Different non-paraxial configurations are plotted in dashed and dotted lines; they are given by formula (32).

the $u_{j,n}(\bar{z}, \bar{\mathbf{r}})$ are smooth functions of their entries ($\bar{z}, \bar{\mathbf{r}}$), and ρ_0 and $\zeta_0 = k_0 \rho_0^2/2$ are the ‘natural’ transverse and longitudinal scales. Substituting this ansatz into Eq. (1) and collecting the terms of similar orders in δ , we get:

Terms of order δ^0 :

$$-\frac{|\mathbf{a}_j|^2}{\rho_0^2} - k_j^2 + k_0^2 = 0,$$

which imposes $k_j = k_0 \sqrt{1 - P^{-2} |\mathbf{a}_j|^2}$.

Terms of order δ^1 :

$$2i \left(\frac{\mathbf{a}_j}{\rho_0^2} \cdot \nabla_{\bar{\mathbf{r}}} + \frac{k_j}{\zeta_0} \partial_{\bar{z}} \right) u_{j,0} + \left(k_0^2 - \frac{|\mathbf{a}_j|^2}{\rho_0^2} - k_j^2 \right) u_{j,1} = 0$$

Terms in $u_{j,1}$ vanish by the definition of k_j . It remains a transport equation whose solution can be written explicitly (remember $\zeta_0 = k_0 \rho_0^2/2$):

$$u_{j,0}(\bar{\mathbf{r}}, \bar{z}) = u_{j,0} \left(\bar{\mathbf{r}} - \frac{2k_0}{k_j} \mathbf{a}_j \bar{z}, 0 \right)$$

The equations obtained by collecting terms with powers δ^n , $n \geq 2$, establish the expression of the corrective term $u_{j,n+1}$ in the form of a transport equation for $u_{j,n+1}$ with a source depending only on $u_{j,n}$. One can then recursively identify all coefficients of the series expansion (34). Thus we have

established that the mode E_j after a propagation distance z has the form (up to terms of order $\delta = \rho_0/r_0$):

$$E_j(z, \mathbf{r}) = \frac{1}{\sqrt{N}} \exp i \left(\frac{\mathbf{a}_j \cdot \mathbf{r}}{\rho_0} + \phi_j(z) \right) g_{j,z/z_0}^{1/2} \left(\frac{\mathbf{r}}{r_0} \right),$$

where $z_0 = k_0 \rho_0 r_0$ and $\phi_j(z)$ is given by (31b). The functions $g_{j,\bar{z}}$ are given by:

$$g_{j,\bar{z}}(\bar{\mathbf{r}}) = g(\bar{\mathbf{r}} - \check{\mathbf{a}}_j \bar{z}),$$

where $\check{\mathbf{a}}_j$ is a rescaled version of \mathbf{a}_j :

$$\check{\mathbf{a}}_j = \frac{\mathbf{a}_j}{\sqrt{1 - P^{-2} |\mathbf{a}_j|^2}},$$

and P is the dimensionless parameter $P = k_0 \rho_0$. Remember that \mathbf{a}_j is normalized so that it is of order 1, so in the paraxial approximation $P \gg 1$ we get $\check{\mathbf{a}}_j = \mathbf{a}_j$.

The total field E is the superposition of the modes E_j . By the arguments developed in Section 4 the 3DAF of the field E is equal to the 3DAF of the mode E_1 . The 3DAF of the field E can then be easily computed:

$$\begin{aligned} \gamma_z(\mathbf{r}, \boldsymbol{\rho}, \zeta) &= \int g \left(\frac{\mathbf{r}}{r_0} - \frac{\mathbf{u}}{\sqrt{1 - P^{-2} |\mathbf{u}|^2}} \frac{z}{z_0} \right) \hat{f}(\mathbf{u}) \\ &\quad \times \exp i \left(\frac{\mathbf{u} \cdot \boldsymbol{\rho}}{\rho_0} + k_0 \zeta \sqrt{1 - P^{-2} |\mathbf{u}|^2} \right) d^2 \mathbf{u}. \end{aligned}$$

As a straightforward application of this formula we can identify the global envelope of the optical intensity $\langle |E|^2(z, \mathbf{r}) \rangle = \gamma_z(\mathbf{r}, \mathbf{0}, 0)$. The shape of the global envelope after propagation over a distance z is the convolution of the initial envelope by a density that is a rescaled version of \hat{f} :

$$\begin{aligned} \langle |E|^2(z, \mathbf{r}) \rangle &= g * \hat{f}_{z/z_0, P}(\mathbf{r}/r_0), \\ \hat{f}_{z, P}(\bar{\mathbf{r}}) &= \frac{\bar{z}^2}{(\bar{z}^2 + P^{-2} |\bar{\mathbf{r}}|^2)^2} \hat{f} \left(\frac{\bar{\mathbf{r}}}{\sqrt{\bar{z}^2 + P^{-2} |\bar{\mathbf{r}}|^2}} \right), \end{aligned}$$

where $*$ stands for the convolution operator.

5.3. The paraxial approximation revisited

We now revisit the above derived results in the framework $P \gg 1$ which corresponds to the paraxial approximation. The 3DAF of the field E then reads:

$$\begin{aligned} \gamma_z(\mathbf{r}, \boldsymbol{\rho}, \zeta) &= \exp(ik_0 \zeta) \int g \left(\frac{\mathbf{r}}{r_0} - \frac{\mathbf{u}}{z_0} \right) \hat{f}(\mathbf{u}) \\ &\quad \times \exp i \left(\frac{\mathbf{u} \cdot \boldsymbol{\rho}}{\rho_0} - \frac{|\mathbf{u}|^2}{4\zeta_0} \right) d^2 \mathbf{u}, \end{aligned}$$

that is the limit of Eq. (35) as $P \rightarrow \infty$. The overall envelope of the intensity distribution of the beam is the convolution of the initial envelope g by a rescaled version of the density \hat{f} :

$$\langle |E|^2(z, \mathbf{r}) \rangle = g * \hat{f}_{z/z_0}(\mathbf{r}/r_0), \tag{35a}$$

$$\hat{f}_z(\bar{\mathbf{r}}) = \frac{1}{\bar{z}^2} \hat{f} \left(\frac{\bar{\mathbf{r}}}{\bar{z}} \right). \tag{35b}$$

If $z = 0$, then \hat{f}_z is the Dirac function at $\bar{\mathbf{r}} = 0$. We shall see in Section 6 a practical application of this formula to the case of super-Gaussian shaped envelope.

The speckle spots also spread out along the propagation and this deformation is governed at the beam center by a convolution of the initial form f by a rescaled version of the function \hat{g} :

$$\gamma_z(\mathbf{r} = \mathbf{0}, \boldsymbol{\rho}) = \hat{g}_{z/z_0} * f(\boldsymbol{\rho}_0/r_0), \tag{36a}$$

$$\hat{g}_z(\bar{\boldsymbol{\rho}}) = \frac{1}{\bar{z}^2} \hat{g} \left(\frac{\bar{\boldsymbol{\rho}}}{\bar{z}} \right). \tag{36b}$$

One can detect a symmetry in the above expressions in the sense that propagation involves a convolution of the inverse Fourier transform of f by g , and reciprocally. That is why the expressions are so simple in the case of Gaussian Schell-model sources, since all functions are Gaussian and are consequently self-similar by convolutions.

6. Application to the focal spot generated by a kinoform phase plate

We shall study in this section a practically relevant configuration, which originally triggered this

work. We shall then be able to quantify very precisely the physically relevant features, and in particular the three-dimensional shape of the focal spot generated by a KPP. In this section we do not assume that the conditions of paraxial approximation are satisfied. We shall revisit and discuss the results when these conditions are satisfied in the next section.

6.1. The field in the focal plane

First we have to compute the field in the focal plane. The experimental configuration is as described in Fig. 5. A monochromatic plane wave source illuminates a random phase plate (RPP), which consists of square elements imposing randomly a phase shift of 0 or π . These elements are labeled by two integer indices (j, l) which are such that $j^2 + l^2 \leq N^2/4$, where $N = D/h$, D is the near field beam aperture, and h is the length of the side of a square element of the RPP. Thus $c_N^2 = [\pi N^2/4]$ is the number of elements of the RPP. We also denote by F the lens focal length. The beamlets generated by the elements focus onto the target; they interfere and form a speckle pattern. The field in the focal plane can be computed by considering the geometric framework depicted in Fig. 6. The distance $d(\mathbf{R}, \mathbf{r})$ can be obtained from the theorem of Pythagoras:

$$(F + d(\mathbf{R}, \mathbf{r}))^2 = |\mathbf{R} - \mathbf{r}|^2 + F^2,$$

which leads to the solution:

$$d(\mathbf{R}, \mathbf{r}) = \sqrt{F^2 + |\mathbf{R} - \mathbf{r}|^2} - F.$$

The lens is assumed to be perfect in the sense that a plane wave is changed into a spherical wave con-

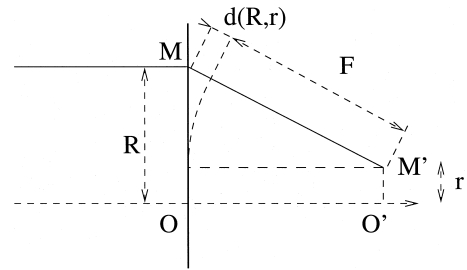


Fig. 6. Geometric configuration showing the lens plane passing through O and the focal plane passing through O'.

verging on the focal point O' at distance F from the lens. Thus the action of the lens is to add the phase $-k_0 d(\mathbf{R}, \mathbf{0})$ to the wave passing through the lens at point M . Accordingly, in the focal plane, the phase mismatch between the points O' and M' is $k_0(d(\mathbf{R}, \mathbf{r}) - d(\mathbf{R}, \mathbf{0}))$:

$$\phi_m(\mathbf{R}, \mathbf{r}) - \phi_m(\mathbf{R}, \mathbf{0}) = -\frac{k_0 \mathbf{R} \cdot \mathbf{r}}{\sqrt{F^2 + |\mathbf{R}|^2}}.$$

Each element of a RPP is squared so that the patterns generated by the beamlets all have the profile of the diffraction function of a square aperture, that is to say an Airy function with radius:

$$r_0 = \frac{\lambda_0 F}{h}. \tag{37}$$

Accordingly the field E_0 in a point $\mathbf{r} = (x, y)$ of the focal plane $z = 0$ is the overlap of c_N^2 elementary fields whose phases are the sums of the phase mis-

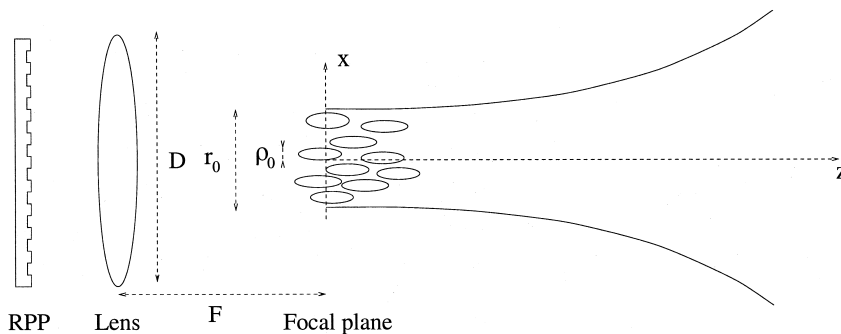


Fig. 5. Schematic view of the generation of a focal spot by a binary Random Phase Plate.

matches $\phi_m(jh, lh, \mathbf{r})$ and of the random phases $\phi_{j,l}$ imposed by the RPP:

$$E_0(\mathbf{r}) = \frac{g(\mathbf{r}/r_0)^{1/2}}{c_N} \sum_{j,l} \exp -i(k_0 d_{j,l}(\mathbf{r}) - \phi_{j,l}), \tag{38a}$$

$$g(\bar{\mathbf{r}}) = I_0 \text{sinc}^2(\bar{x}) \text{sinc}^2(\bar{y}), \tag{38b}$$

where

$$d_{j,l}(\mathbf{r}) = \frac{(jx + ly)h}{\sqrt{F^2 + (j^2 + l^2)h^2}}$$

If N^2 is large, the field E_0 is a Gaussian process by the central limit theorem. The field can be expressed into the standard modal representation if one chooses \mathbf{a} of the form:

$$\mathbf{a}_{j,l} = \frac{k_0 \rho_0}{\sqrt{F^2 + (j^2 + l^2)h^2}} (jh, lh),$$

where the (j, l) 's are uniformly distributed over the disc $B(0, N/2)$. Denoting by ρ_0 the correlation radius:

$$\rho_0 = \frac{\lambda_0 F}{D}, \tag{39}$$

this also writes as:

$$\mathbf{a} = \frac{\mathbf{v}}{\sqrt{1 + P^{-2}|\mathbf{v}|^2}}, \tag{40}$$

where $P = k_0 \rho_0$ and \mathbf{v} is uniformly distributed over $B(0, \pi)$. Thus, after the change of variable $\mathbf{u} = \mathbf{v}/\sqrt{1 + P^{-2}|\mathbf{v}|^2}$:

$$\hat{f}(\mathbf{u}) = \pi^{-3} (1 - P^{-2}|\mathbf{u}|^2)^{-2} \chi_{B(0, \pi/\sqrt{1+P^{-2}\pi^2})}(\mathbf{u}).$$

The degree of coherence is obtained by an inverse Fourier transform:

$$f(\bar{\boldsymbol{\rho}}) = \frac{2}{\pi^2} \int_0^\pi \frac{\sqrt{1+(\pi/P)^2}}{\sqrt{1+(\pi/P)^2}} J_0(s|\bar{\boldsymbol{\rho}}|) \frac{s}{(1 - P^{-2}s^2)^2} ds. \tag{41}$$

In the paraxial case ($P \gg 1$):

$$f(\bar{\boldsymbol{\rho}})|_{\text{parax}} = \frac{2J_1(\pi|\bar{\boldsymbol{\rho}}|)}{\pi|\bar{\boldsymbol{\rho}}|}. \tag{42}$$

Note that in terms of the so-called F-number $F_\# := 2F/D$, the parameter P writes: $P = \pi F_\#$. Compar-

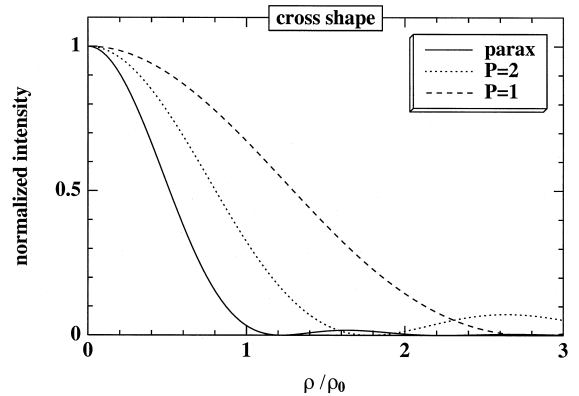


Fig. 7. Normalized cross shape of the intensity profile of a speckle spot in the RPP configuration. The paraxial configuration is plotted in solid line; it corresponds to the limit case $P \rightarrow \infty$ and is given by formula (42). Different non-paraxial configurations are plotted in dashed and dotted lines.

ing the curves plotted in Fig. 7 it appears that the paraxial approximation tends to reduce the true cross radius of the speckle spots.

In case of a RPP, the elements of the phase plate are squared so that the overall envelope is an Airy function with radius $r_0 = \lambda_0 F/h$. In case of a KPP, the result is the same but the overall envelope is no more an Airy but a super-Gaussian function. From now on we shall consider that the envelope of the focal spot in the focal plane has super-Gaussian shape with power n and radius r_0 . The CAF of the field in the focal plane $z = 0$ is then given by:

$$\gamma_0(\mathbf{r}, \boldsymbol{\rho}) = I_0 \exp\left(-\frac{|\mathbf{r}|^n}{r_0^n}\right) \times f\left(\frac{\boldsymbol{\rho}}{\rho_0}\right). \tag{43}$$

6.2. Propagation beyond the focal plane

The 3DAF is given by Eq. (35) with $\hat{f}(\mathbf{u})$ given by (40) and $g(\bar{\mathbf{r}}) = I_0 \exp -|\bar{\mathbf{r}}|^n$. This expression permits to compute closed-form expressions for the longitudinal shape of the speckle spots and for the shape of the global envelope out of the focal plane.

The longitudinal shape of the speckle spots is imposed by the form of the 3DAF in the ζ -direction.

$$|\gamma_{z=0}(\mathbf{r}, \boldsymbol{\rho}, \zeta)|^2 = \frac{4P^4 I_0^2}{\pi^4} \left| \int_0^1 \frac{1}{\sqrt{1+(\pi/P)^2}} \exp\left(i \frac{P^2 \zeta}{2 \zeta_0} s\right) \frac{ds}{s^3} \right|^2.$$

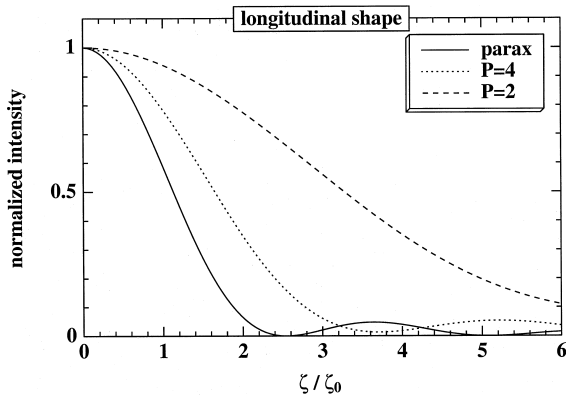


Fig. 8. Normalized longitudinal shape of the intensity profile of a speckle spot in the RPP configuration. The paraxial configuration is plotted in solid line; it corresponds to the limit case $P \rightarrow \infty$ and is given by formula (33). Different configurations are plotted in dashed and dotted lines.

Remember that within the paraxial approximation this function is given by (33). Comparing the curves plotted in Fig. 8 it appears that the paraxial approximation tends to reduce the true longitudinal length of the speckle spots. This is not in contradiction with the conclusion derived in Section 5.2, since the main nonparaxial effect in the KPP configuration is to modify the cross shapes of the speckle spots, which were given as initial data in Section 5.2.

The evolution of the shape of the global envelope is governed by the convolution described in Section 5.2:

$$\langle |E|^2(z, \mathbf{r}) \rangle = g * \hat{f}_{z/z_0, P}(\mathbf{r}/r_0),$$

$$\hat{f}_{z, P}(\bar{\mathbf{r}}) = \frac{\bar{z}^2}{(\bar{z}^2 + P^{-2}|\bar{\mathbf{r}}|^2)^2} \hat{f}\left(\frac{\bar{\mathbf{r}}}{\sqrt{\bar{z}^2 + P^{-2}|\bar{\mathbf{r}}|^2}}\right).$$

Substituting the expression (40) of \hat{f} , we finally get that:

$$\hat{f}_{z, P}(\bar{\mathbf{r}}) = \pi^{-3} \bar{z}^{-2} \chi_{B(0, \pi \bar{z})}(\bar{\mathbf{r}}).$$

We then come to the surprising conclusion that the parameter P does not come into this expression, that is to say the result that is obtained by applying the paraxial approximation is correct even if the conditions of paraxial approximation are not fulfilled. In conclusion, the paraxial approximation makes the cross (resp. longitudinal) shapes of the speckle spots narrower (resp. larger) than they are actually. Never-

theless the shape of the global envelope predicted by the paraxial approximation is correct.

7. The KPP case: discussion

Throughout this section we shall assume that the paraxial approximation holds true in the sense that $\rho_0 \gg \lambda_0$ or equivalently $D \ll F$. We shall revisit some of the results derived in Section 6 and discuss their implications for ICF. As pointed out in Section 6 the results concerning the overall envelope are valid even if the condition $D \ll F$ of paraxial approximation is not fulfilled.

7.1. Rayleigh distance

The so-called Rayleigh distance is defined as the length z which corresponds to a decay by a factor 2 of the optical intensity at the beam center. The optical intensity at $\mathbf{r} = \mathbf{0}$ can be deduced from Eq. (35a):

$$\langle |E|^2(z, \mathbf{0}) \rangle = I_0 M_n(z/z_0), \tag{44}$$

where $M_n(\bar{z}) = \pi^{-2} \bar{z}^{-2} \int_0^{\pi^2 \bar{z}^2} \exp -u^{n/2} du$ and $z_0 = k_0 \rho_0 r_0$. The function M_n is plotted in Fig. 9 for different powers n . The Rayleigh distance is found to be equal to: $z_R(n) = \alpha_n z_0$, with in particular $\alpha_2 \approx 0.401$, $\alpha_4 \approx 0.420$, $\alpha_6 \approx 0.427$ and $\alpha_\infty = \sqrt{2} / \pi \approx 0.450$. It thus appears that this distance is only very slightly dependent on the power n . Indeed, as shown by Fig. 9, the larger n , the more

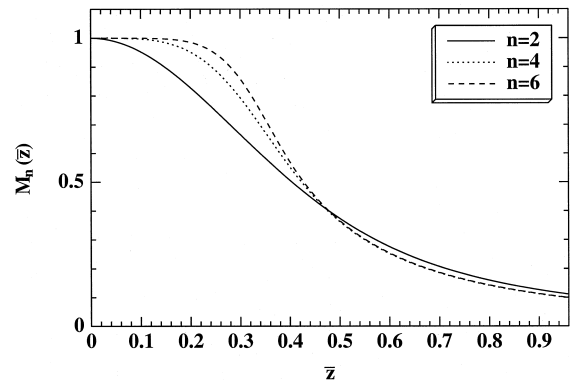


Fig. 9. Normalized mean intensity at the beam center versus the propagation distance for different values of the power n ($\bar{z} = z/z_0$).

stable the mean intensity at the beam center is for propagation distances smaller than z_0/π . However, beyond this distance and whatever the power n , the mean intensity at the beam center decays at a very similar rate. When $n \rightarrow \infty$, that is to say in case of a flat-top envelope, the function M_∞ is of the form $M_\infty(\bar{z}) = \min(1, \pi^{-2} \bar{z}^{-2})$.

7.2. Overall envelope

The Rayleigh distance, and more generally speaking the behavior of the optical intensity at the beam center, is not as relevant as one can expect, in that it does not contain the whole information about the evolution of the global envelope, which may evolve very differently according to the value of the power n . Let us now examine the deformation of the cross shape of the envelope along the propagation. By applying the formula (35a) we get that the overall envelope is convoluted by a density that is a rescaled version of the inverse Fourier transform of f :

$$\langle |E|^2(z, \mathbf{r}) \rangle = I_0 \left(\exp(-|\cdot|^n) * \hat{f}_{z/z_0}(\cdot) \right) (\mathbf{r}/r_0), \tag{45a}$$

$$\hat{f}_z(\bar{\mathbf{r}}) = \pi^{-3} \bar{z}^{-2} \chi_{B(0, \pi \bar{z})}(\bar{\mathbf{r}}). \tag{45b}$$

By considering Fig. 10 and Fig. 11, which plot the intensity profiles of the global envelope after differ-

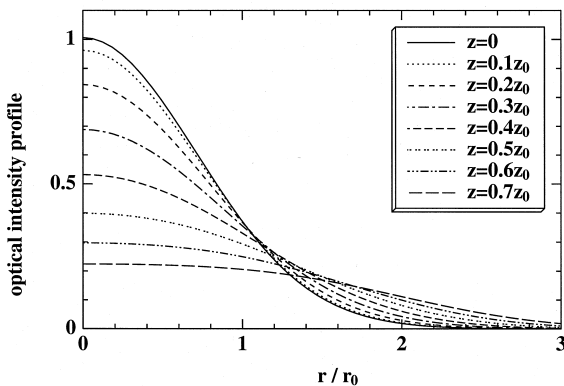


Fig. 10. Normalized global envelope of the beam ($I_0 = 1$) at different propagation distances $0.1 m z_0, m = 0, \dots, 7$ - Case of an initially Gaussian envelope $n = 2$.

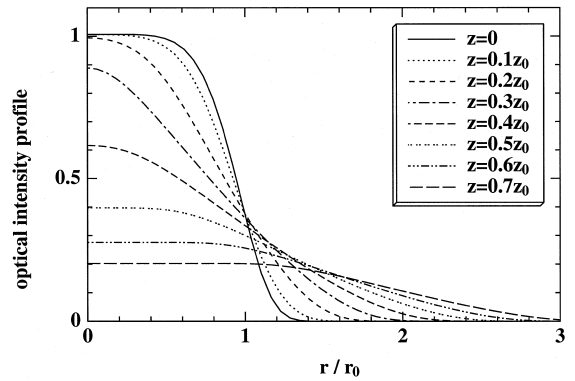


Fig. 11. Normalized global envelope of the beam ($I_0 = 1$) at different propagation distances $0.1 m z_0, m = 0, \dots, 7$ - Case of an initially super-Gaussian envelope with power $n = 6$.

ent propagation distances, one can observe that the edges of the focal spot, which used to be sharp in the focal plane $z = 0$ in the super-Gaussian case, drastically collapse. This phenomenon is much more noticeable than the decay of the intensity at the beam center, which actually occurs after the collapse of the edges.

7.3. Speckle radius

Let us now focus our attention to the evolution of the fast-varying fluctuations of the speckled field along the propagation. The CAF can be computed by

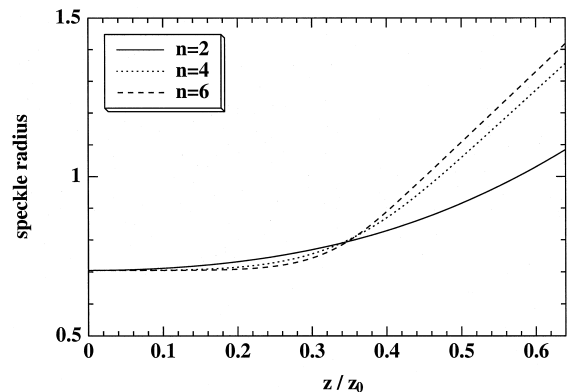


Fig. 12. Normalized speckle radius (i.e. divided by ρ_0) of the beam along the z -axis for different values of the power n .

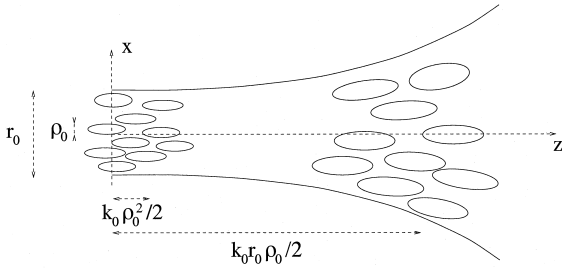


Fig. 13. Main characteristic distances relative to the propagation of a partially coherent beam.

setting $\zeta = 0$ in Eq. (35). At the beam center the CAF writes:

$$\gamma_z(\mathbf{r} = \mathbf{0}, \rho) = \frac{I_0}{\pi_3} \int_{B(0, \pi)} \exp\left(-\left|\frac{z\mathbf{u}}{z_0}\right|^n + i\frac{\mathbf{u} \cdot \boldsymbol{\rho}}{\rho_0}\right).$$

Let us now consider the behavior of γ as a function of $\boldsymbol{\rho}$, which gives the intensity profiles of the hot spots according to Adler's results (see Eq. (10)). An efficient way to characterize this behavior is to map out the evolution of the speckle radius of the beam along the propagation. The speckle radius at the beam center can be defined as the length ρ_c for which the CAF satisfies $\gamma_z(\mathbf{0}, \rho_c \hat{\mathbf{e}}) = (1/2)\gamma_z(\mathbf{0}, \mathbf{0})$, where $\hat{\mathbf{e}}$ is any unitary vector. By plotting the evolution of the so-defined speckle radius (Fig. 12), one can put into evidence the following features. The speckle radius looks stable while $z < z_0/\pi$, and this is all the more true as the initial overall envelope is super-Gaussian. Once the critical distance z_0/π is reached, the speckle radius rapidly increases, which means that the hot spots spread out as the envelope does. In the limit case $n \rightarrow \infty$, the function $z \mapsto \rho_c(z)$ is simply: $\rho_c(z) = \beta_c \rho_0 \max(1, \pi z/z_0)$, where $\beta_c \approx 0.705$ is such that $f(\beta_c) = 1/2$.

8. Conclusion

The propagation of a speckle pattern with beam radius r_0 and correlation radius $\rho_0 \ll r_0$ can be characterized by two distances $\zeta_0 = k_0 \rho_0^2/2$ and $z_0 = k_0 \rho_0 r_0$:

ζ_0 is the length of the speckle spots in the z -direction. The statistical properties of the fast-vary-

ing fluctuations of the field (and in particular the sizes of the speckle spots) and the global shape of the beam (and in particular the global radius) are not modified for propagation distances of the order of ζ_0 .

The statistical properties of the fast-varying fluctuations and the global shape of the beam evolve at the scale z_0 . The overall envelope is given by the convolution of the input envelope by a rescaled version of the inverse Fourier transform of the input degree of coherence. Similarly the shape of the speckle spots is given the convolution of the input degree of coherence by a rescaled version of the inverse Fourier transform of the overall envelope.

Our conclusions and formulas can be applied to the KPP configuration, and more generally they hold true as soon as the two following conditions are fulfilled: First the field obeys Gaussian statistics. Second the global radius r_0 is large compared with the wavelength λ_0 and with the correlation radius ρ_0 .

Acknowledgements

We thank A. Migus and C. Rouyer for useful and stimulating discussions. This work was performed under the auspices of the Laser MegaJoule Program of Commissariat à l'Énergie Atomique/Direction des Applications Militaires (grant CEA/DAM No. 9V 1665 YB F7).

References

- [1] O. Kinrot, I.S. Averbukh, Y. Prior, Phys. Rev. Lett. 75 (1995) 3822.
- [2] D. Huang, E.A. Swanson, C.P. Lin, J.S. Schuman, W.G. Stinson, W. Chang, M.R. Hee, T. Flotte, K. Gregory, C.A. Puliafito, J.G. Fujimoto, Science 254 (1991) 1178.
- [3] R.H. Lehmborg, S.P. Obenschain, Opt. Commun. 46 (1983) 27.
- [4] R.H. Lehmborg, A.J. Schmitt, S.E. Bodner, J. Appl. Phys. 62 (1987) 2680.
- [5] J.D. Lindl, R.L. McCrory, E.M. Campbell, Phys. Today 45 (1992) 32.
- [6] S.N. Dixit, I.M. Thomas, B.W. Woods, A.J. Morgan, M.A. Hennesian, P.J. Wegner, H.T. Powell, Appl. Opt. 32 (1993) 2543.
- [7] S.N. Dixit, M.D. Feit, M.D. Perry, H.T. Powell, Opt. Lett. 21 (1996) 1715.
- [8] M. André, in: J. Coutant (Ed.), the French program for ICF,

- presented at the Technical Committee Meeting on Drivers and Ignition Facilities for Inertial Fusion, Paris, France, CEA/DAM Publications, Limeil-Valenton, France, 1995.
- [9] J.E. Rothenberg, *J. Opt. Soc. Am. B* 14 (1997) 1664.
- [10] L. Mandel, E. Wolf, *Optical Coherence and Quantum Optics*, Cambridge University Press, Cambridge, UK, 1995.
- [11] A.T. Friberg, R.J. Sudol, *Opt. Commun.* 41 (1982) 383.
- [12] F. Gori, *Opt. Commun.* 46 (1983) 149.
- [13] P. De Santis, F. Gori, G. Guattari, C. Palma, *Opt. Commun.* 29 (1979) 256.
- [14] R. Simon, N. Mukunda, *J. Opt. Soc. Am. A* 10 (1993) 95.
- [15] F. Gori, G. Guattari, C. Padovani, *J. Opt. Soc. Am. A* 3 (1987) 311.
- [16] F. Gori, M. Santarsiero, R. Borghi, S. Vicalvi, *J. Mod. Opt.* 35 (1998) 539.
- [17] J.D. Kilkenny, S.G. Glendinning, S.W. Haan, B.A. Hammel, J.D. Lindl, D. Munro, B.A. Remington, S.V. Weber, J.P. Knauer, C.P. Verdon, *Phys. Plasmas* 1 (1994) 1379.
- [18] A. Papoulis, *Systems and Transforms and Applications in Optics*, McGraw Hill, New York, 1968.
- [19] J.W. Goodman, Statistical properties of laser speckle patterns, in: J.C. Dainty (Ed.), *Laser Speckle and Related Phenomena*, Topics in Applied Physics 9, Springer-Verlag, Berlin, 1984, pp. 9–75.
- [20] J. Garnier, C. Gouédard, L. Videau, A. Migus, *J. Opt. Soc. Am. A* 14 (1997) 1928.
- [21] J. Adler, *The Geometry of Random Fields*, Wiley, New York, 1981.
- [22] D. Middleton, *Introduction to Statistical Communication Theory*, McGraw Hill, New York, 1960, p. 141.
- [23] M.J. Bastiaans, *J. Opt. Soc. Am. A* 3 (1986) 1227.
- [24] J. Paye, A. Migus, *J. Opt. Soc. Am. B* 12 (1995) 1480.